Formation of a Complete Solid Solution between the Triphylite and Fayalite Olivine Structures

N. Recham,[†] M. Casas-Cabanas,[‡] J. Cabana,[§] C. P. Grey,[§] J-C. Jumas,[||] L. Dupont,[†] M. Armand,[†] and J-M. Tarascon*,[†]

LRCS, UMR 6007, Université de Picardie Jules Verne, 80039 Amiens, France, EMAT, University of Antwerp, Groenenborgerlaan 171, B-2020 Antwerp, Belgium, Department of Chemistry, SUNY at Stony Brook, Stony Brook, New York, 11794-3400, and LAMMI, UMR 5072, Université Montpellier II, 34095 Montpellier, France

Received July 4, 2008. Revised Manuscript Received August 28, 2008

The recent infatuation for $LiFePO_4$ as positive electrode material in Li-ion batteries has prompted a renewed interest in olivine-type structures, with a view to enhance their conduction properties. We show that the dual substitution of Li for Fe and of P for Si in the olivine $LiFePO_4$ phase leads to a complete solid solution $Li_{1-x}Fe_{1+x}P_{1-x}Si_xO_4$ as deduced from combined X-ray diffraction, Mössbauer, and NMR experiments. Our findings challenge the common belief that the anionic network cannot be substituted. Moreover, it is found that such a substitution promotes Li intersite mixing between the olivine M1 and M2 sites. Such mixing, together with the worsening of the conducting properties of the dually substituted samples, is believed to be responsible for the poor electrochemical performances of the member's series. Beyond $x = 0.20$, the samples were electrochemically inactive. While the current materials are disappointing application-wise, such a study provides clues to the rich chemistry remaining to be unveiled with olivine-type structures in particular and polyanionic compounds in general.

Introduction

One important requirement for the progress of our society toward increased environmental sustainability is, among a wide range of issues, the development of high performing, abundant, safe, and low-cost high-energy-density materials for use in lithium-ion batteries (LIBs). As part of this, new positive insertion electrode materials are required, so as to improve the LIB technology, which is powering most of today's portable electronics, and is on the verge of penetrating the electric automotive market. Despite more than 20 years of research for Li-ion insertion/deinsertion compounds the harvest has been very limited,[1] and the number of attractive candidates can still be counted on the fingers of one hand: the layered-type $LiCoO_2$ oxides and derivatives based on $LiMn_{1/3}Ni_{1/3}Co_{1/3}O_2$, the 3D spinel $LiMn_2O_4$ compounds, and the latest to come onto the scene and create great excitement in the battery and wider community, the olivine $LiFePO_4$ phase[2] (hereafter called LFP).

In contrast to conventional wisdom, the flat potential of the LFP electrode (two-phase system) is not an advantage for the management of series-connected devices due to its more complex electronic requirement (which necessitates keeping count of the total charge passed in the cell). Although nanoparticles of LFP show two nonstoichiometric domains at each end of the charge curve, $Li_{1-\alpha}FePO_4$ and $Li_\beta FePO_4$, the middle domain is still flat; furthermore, nanoparticles favor high power batteries, but their volumetric capacity can be low due to their low packing density. Interestingly enough, the $Li_{1-\alpha}FePO_4-Li_\beta FePO_4$ system becomes single-phase above 250 °C[3] showing that the energy driving the phase separation is not large.

No clear-cut evidence exists for the replacement of the cations, either on Fe or Li sites, with aliovalent species (Nb^{5+}),[4] but rather this substitution promotes the formation of electronic conductors such as Fe_2P.[5] With "bystander species" like Mg substituting for Fe, the conductivity of $LiFe_{1-x}M_{1-x}PO_4$ (where M could also be Li, Na, K)[6] is likely enhanced, either for Li^+ or e^-; however, as relatively high fractions are needed, this is at the expense of the capacity as the cationic substitution results in a proportional loss in specific capacity. In contrast, the partial or full substitution of Fe for other 3d-metals (Mn, Co, Ni) [6,7] is feasible leading eventually to the isostructural $LiMnPO_4$, $LiCoPO_4$, and $LiNiPO_4$ olivine-type compounds, which in turn show higher redox potentials (4.2, 4.8, and 5 V vs $Li^+/Li°$, respectively) than $LiFePO_4$. They also have poor electronic conductivity and other issues, especially $LiMnPO_4$, which shows a Jahn−Teller distortion in the delithiated form. The latter

* Corresponding author. E-mail: jean-marie.tarascon@sc.u-picardie.fr.
[†] Université de Picardie Jules Verne.
[‡] University of Antwerp.
[§] SUNY at Stony Brook.
[||] Université Montpellier II.

(1) Tarascon, J. M.; Armand, M. *Nature* **2001**, *414*, 359–367.
(2) Padhi, A. K.; Nanjundaswamy, K. S.; Goodenough, J. B. *J. Electrochem. Soc.* **1997**, *144*, 1188–1194.
(3) Delacourt, C.; Poizot, P.; Tarascon, J. M.; Masquelier, C. *Nat. Mater.* **2005**, *4*, 254–260.
(4) Chung, S. Y.; Bloking, J. T.; Chiang, Y. M. *Nat. Mater.* **2002**, *1*, 123–126.
(5) Huang, H.; Yin, S. C.; Nazar, L. F. *Electrochem. Solid State Lett.* **2001**, *4*, A170−A172.
(6) Morgan, D.; Van der Ven, A.; Ceder, G. *Electrochem. Solid State Lett.* **2004**, *7*, A30−A32.
(7) Yamada, A.; Chung, S. C. *J. Electrochem. Soc.* **2001**, *148*, A960−A967.

10.1021/cm801817n CCC: $40.75
Published on Web 10/22/2008

handicap makes its full use difficult even in the presence of carbon coating.[8] Besides, all three require electrolytes that are highly stable against oxidation.

Anionic substitution has not been reported in LFP, and as shown below, is not straightforward. There are, however, other structures involving SiO_4 tetrahedra, such as $Li_2Fe(Mn)SiO_4$ [9−12] and the fluorophosphate $Na(Li)_2FePO_4F$,[13] but they have different structures; the former with an unfavorable fourfold coordination for all the cations, the latter with a lower specific capacity due to an increase in the equivalent weight. The advantage of the latter research involving anion substitution is that a large fraction of the phosphate tetrahedra could be substituted without affecting the Li and Fe contents, thus preserving the capacity. Bearing this in mind, we first looked for new representatives within the family of olivine-type scaffold structures and investigated the $LiFePO_4/Fe_2SiO_4$ system. We found, as reported herein, that the entire $[Li_{1-x}Fe_{1+x}P_{1-x}Si_xO_4]$ ($0 < x < 1$) solid solution can be prepared. For reasons of clarity, the paper will be organized as follows. The synthesis/structural characterization of the solid solution will be first described separately, and afterward the electrochemical performances of the system will be reported.

Experimental Section

Characterization. The X-ray powder diffraction patterns were recorded on a Scintag diffractometer (Cu Kα radiation $\lambda = 1.5418$ Å) or on a Bruker D8 diffractometer using Co Kα radiation ($\lambda_1 = 1.78919$ Å, $\lambda_2 = 1.79321$ Å), equipped with a Gobel mirror and Braun PSD detector, or a Bruker D8 Advance diffractometer (Cu Kα radiation, $\lambda_1 = 1.54053$ Å; $\lambda_2 = 1.54431$ Å), equipped with a linear Vantec counter. Neutron diffraction data were recorded at high resolution on a D1A diffractometer ($\lambda_1 = 1.91$ Å) at the Institute Laue Languevin (ILL, Grenoble, France). Lattice parameters were obtained from full pattern matching refinements via the program Fullprof[14] using the pseudo-Voigt profile function of Thompson et al.[15] The structures of the different phases encountered during this study were refined using the Rietveld method with the Fullprof program. The morphology of the samples was observed with field emission gun scanning electron microscopy (FEI Quanta 200F). The electron microscopy images and nanoprobe EDS analysis, performed to determine the Fe/P:Si ratios, were taken with a FEI Tecnai F20-WTIN instrument fitted with EDAX.

^{57}Fe Mössbauer spectra were recorded in transmission geometry in the constant acceleration mode and with a ^{57}Co(Rh) source of nominal activity of 925 MBq. The velocity scale (±4 mm/s) was calibrated at room temperature with α-Fe foil. The absorbers were prepared from 50 mg of powder mixed with Apiezon grease. The hyperfine parameters δ (isomer shift) and ΔE_q (quadrupole splitting) were determined by fitting Lorentzian lines to the experimental data, using the MOSFIT program. Isomer shift values are given with respect to that of α-Fe.

^{7}Li and ^{31}P MAS NMR experiments were performed with a double-resonance 1.8 mm probe, built by A. Samoson and co-workers (KBFI, Tallinn, Estonia), on a CMX-200 spectrometer using a magnetic field of 4.7 T, at a spinning frequency of 38 kHz, and using a rotor-synchronized spin−echo sequence ($\pi/2-\tau-\pi-\tau-$aq). The ^{7}Li spectra were collected at an operating frequency of 77.71 MHz, with a 2.75 μs $\pi/2$ pulse width and an acquisition delay of 0.2 s. One M LiCl (at 0 ppm) was used as an external reference. In the case of the ^{31}P data, the observed signals were very broad; therefore, the whole spectrum could not be excited simultaneously. To overcome this issue, separate spectra were acquired as a function of irradiation frequency, starting at a carrier frequency of 80.94 MHz, which corresponds to the Larmor frequency of the reference (H_3PO_4). The carrier frequency was moved in steps of 650 kHz, and the resulting spectra were normalized to the same scan number and mathematically added to yield the full spectrum. At each frequency, a $\pi/2$ pulse width of 2.6 μs and 0.1 delay time was used. A solution of H_3PO_4 (0 ppm) was used as an external reference.

Electrochemical tests were performed as follows: positive electrodes were prepared by mixing 85 wt % of active material with 15 wt % SP carbon, as the electronic conductor. Swagelok-type cells were assembled in an argon-filled glovebox with about 10 mg of the material/carbon mix separated from the negative electrode (lithium foil) by two sheets of fiberglass disks, the whole being soaked in a $LiPF_6$ (1 M) solution of ethylene carbonate (EC)/dimethyl carbonate (DMC) mixture (1:1, v/v). An aluminum current collector was used as the positive side to avoid electrolyte decomposition at high potential. Galvanostatic tests were conducted with a Mac-Pile controller at a constant temperature of 25 °C unless otherwise specified.

Synthesis. $[Li_{1-x}Fe_{1+x}P_{1-x}Si_xO_4]$ ($0<x<1$) samples were prepared from $LiFePO_4$ and Fe_2SiO_4 powders, via a ceramic route.

$LiFePO_4$. Highly divided $LiFePO_4$ was first prepared via a hydrothermal process by reacting at 180 °C for 5 h stoichiometric amounts of $LiOH\cdot H_2O$ (99.5%), $FeSO_4\cdot 7H_2O$ (99%), and H_3PO_4 (85%).

Fe_2SiO_4. This was prepared under argon at 750 °C for 24 h in an arc-welded stainless steel tube, from Fe_2O_3, Fe metal, and SiO_2 powders according to the following reaction: $(2/3)Fe_2O_3 + (2/3)Fe^0 + SiO_2 = Fe_2SiO_4$. For improved reactivity, nanometric Fe_2O_3 powders were synthesized from commercial dehydrated Fe(II) oxalate ($FeC_2O_4\cdot 2H_2O$) by calcination under air at 400 °C for 10 h. For the same reason SiO_2 nanopowders were prepared via hydrolysis of tetraethoxysilane (TEOS) in a water−ethanol (1−5) mixture and one drop of ammonia as catalyst to promote room temperature precipitation. Once recovered the precipitate was heated to 400 °C for 2 h to eliminate the remaining water. Last, stoichiometric amounts of Fe_2O_3, SiO_2, and Fe powders were thoroughly ball-milled for 0.5 h, under Ar atmosphere and using a SPEX 8000 shock-miller, in a 10 mL cell with a ball/powder ratio of 4. Afterward the powders were placed in a stainless steel tube sealed under argon; the tube was annealed at 750 °C for 24 h to produce pure Fe_2SiO_4 powders.

Finally, preweighed stoichiometric amounts of the aforementioned $(1-x)LiFePO_4$ and xFe_2SiO_4 powders (with $x = 0.07, 0.15,$

(8) Ravet, N.; Goodenough, J. B.; Besner, S.; Simoneau, M.; Hovington, P.; Armand, M. Improved iron-based cathode material. *196th Meeting of the Electrochemical Society*, Abstract no. 127, Hawaii, 1999; The Electrochemical Society Publisher: Pennington, NJ, 1999. Armand, M.; Gauthier, M.; Magnan, J.-F.; Ravet, N. World Patent WO 02/27823 A1, 1999.
(9) Nyten, A.; Abouimrane, A.; Armand, M.; Gustafsson, T.; Thomas, J. O. *Electrochem. Commun.* **2005**, *7* (2), 156–160.
(10) Dominko, R.; Bele, M.; Gaberscek, M.; Meden, A.; Remskar, M.; Jamnik, J. *Electrochem. Commun.* **2006**, *8* (2), 217–222.
(11) Arroyo-de Dompablo, M. E.; Armand, M.; Tarascon, J. M.; Amador, U. *Electrochem. Commun.* **2006**, *8* (8), 1292–1298.
(12) Arroyo-de Dompablo, M. E.; Gallardo-Amores, J. M.; Gracia-Martinez, J.; Moran, E.; Tarascon, J. M.; Armand, M. *Solid State Ionics* **2008**, in press.
(13) Ellis, B. L.; Makahnouk, W. R. M.; Makimura, Y.; Toghill, K.; Nazar, L. F. *Nat. Mater.* **2002**, *1*, 123–126.
(14) Rodríguez-Carvajal, J. *CPD Newsletter* **2001**, *26*, 12 (Recent Developments of the Program FULLPROF, available at http://www.iucr.org/iucr-top/news/index.html; the program and documentation can be obtained from http://www.ill.fr/dif/Soft/fp).
(15) Thompson, P.; Cox, D. E.; Hastings, J. B. *J. Appl. Crystallogr.* **1987**, *20*, 79–83.

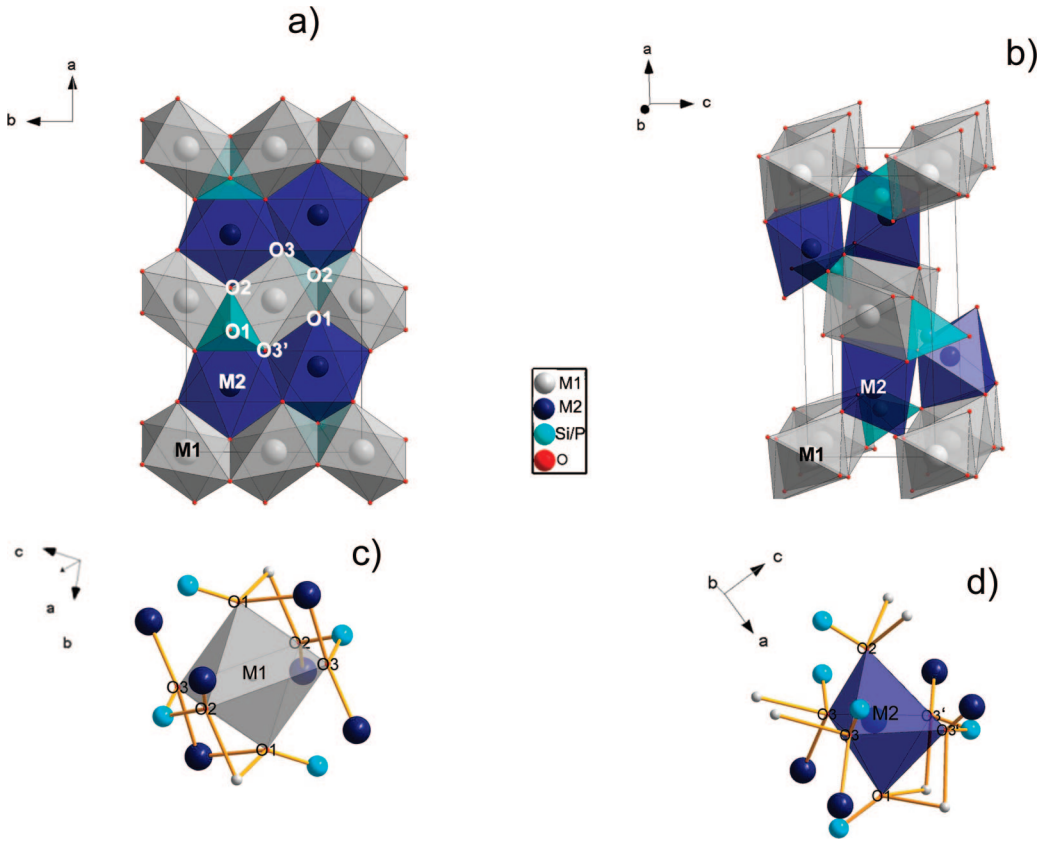

Figure 1. Polyhedron representation of the olivine structure along the *c* axis (a) showing the different types of occupied positions. The same structure viewed along the *b* axis (b) where the interconnections between the different types of polyhedra become clearly visible. Local geometry of M1 (c) and M2 (d) octahedral sites, respectively, with first and second coordination spheres, in which the extreme distortion of M2 octahedron can clearly be appreciated.

0.25, 0.35, 0.50, and 0.75) were placed in a stainless steel milling container and ball milled for 30 min under Ar atmosphere using a SPEX; the resulting mixture was placed in a sealed pure iron tube, which was itself disposed into an evacuated sealed quartz glass (i.e., to prevent Fe oxidation) and heated at a rate of 4 °C/min to 980 °C for 48 h, the furnace was turned off, and the mixture was left to cool down to room temperature. Use of stainless steel resulted in the apparition of Fe^0 due to the reducing power of Cr in the alloy. The resulting brownish-green samples were ground to form powders prior to characterizing the structural/textural aspects by XRD, microscopy, and Mössbauer and NMR experiments.

Results

$Li_{1-x}Fe_{1+x}P_{1-x}Si_xO_4$ ($0 \leq x \leq 1$) solid solutions were synthesized in a sealed iron tube from ball-milled LFP and homemade Fe_2SiO_4 precursors. Attempts to synthesize the Fe_2SiO_4 precursor from micrometer-sized commercial precursors (including fumed silica) always failed resulting in multiphase products. Therefore, we used nanoparticles of both SiO_2 and Fe_2O_3 as starting materials. Similar solid solutions could also be obtained up to $x = 0.3$, by performing the heating step in air in a covered graphite crucible using a flash heating, that is to say, by placing the crucible directly in an oven preheated at 980 °C for 20 min only. Longer reaction times (>30 min) or shorter ones (<10 min) together with different annealing temperatures were shown to lead to multiphase samples consisting of both end member phases plus hints of the solid solution phases, as discussed later. As an alternative synthesis we experienced the feasibility to prepare similar solid solutions by arc melting pellets made of stoichiometric amounts of ball-milled $LiFePO_4$ and Fe_2SiO_4 powders. However, for reasons of length, the data will only be reported for the samples made in sealed iron tubes.

Structural Characterization. The two end members of the $Li_{1-x}Fe_{1+x}P_{1-x}Si_xO_4$ ($0 \leq x \leq 1$) solid solution are Fayalite ($x = 1$) and Triphylite ($x = 0$). Fayalite belongs to the olivine group and can be described as a slightly distorted hexagonal close-packed oxygen array resulting in an orthorhombic structure (space group *Pnma*). The key structural unit of the olivine structure is an array of serrated chains of MO_6 edge sharing octahedra lying parallel to the *b* axis (Figure 1a), where only half of the octahedral voids are occupied (M1 sites, 4a Wyckoff position, on the inversion center). These chains are linked together by silicon-centered tetrahedra sharing a triangle of edges with the octahedra from one serrated chain and the opposite vertex with the vertex of three octahedra belonging to the chain displaced at distance *c* from the first one. Additionally, these layers are connected to the ones displaced by *c*/2 (where the occupied serrated chain lies directly above the unoccupied serrated chain of the first layer) by vertex and edge sharing of a second type of octahedra (M2 sites, 4c Wyckoff position, on the mirror plane) (Figure 1b). The result is a structure with rather distorted cationic sites due to electrostatic repulsions. In the M1 octahedron all the oxygen atoms belong to shared edges resulting in more regular cation−oxygen distances than those in M2 as displayed in Figure 1c,d, respectively. In the latter and in the Si tetrahedron, the longest

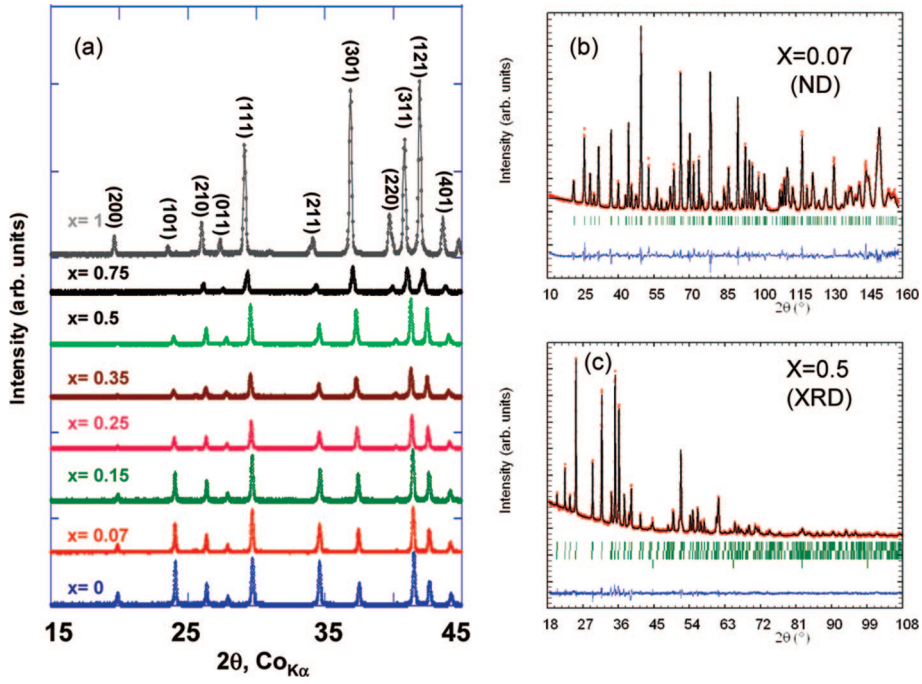

Figure 2. XRD diffraction patterns for the various members of the series are shown in a. Together with the $Li_{1-x}Fe_{1+x}P_{1-x}Si_xO_4$ series shown in a is (b and c) the experimental neutron and X-ray powder diffraction pattern (dotted curve), respectively, compared to the Rietveld-refined profile (continuous line) and difference curve (blue).

bonds correspond to oxygen atoms forming shared edges while the cation−oxygen distances of nonshared edges exhibit variations in length resulting not only from electrostatic repulsions but also from spatial factors. In Fayalite ($x = 1$) both M1 and M2 sites are occupied by Fe atoms. The average Fe−O distances are 2.159 Å for M1 and 2.178 Å for M2, and the Si−O average distance is 1.620 Å.[16] The structure of Triphylite is basically the same, with P occupying tetrahedral positions and half of the Fe atoms being substituted by Li. Although the ionic radii of Li^{1+} and Fe^{2+} are very similar, the more stable configuration corresponds to Li in M1 sites, in agreement with the third Pauling rule for which the positions with more shared edges will be more stable for smaller charges (although it may happen that they substitute for one another to some extent).[17,18] The overall unit cell is smaller and more distorted from regular close-packing than in Fayalite mainly due to the smaller ionic radii of P ($r = 0.17$ Å) and Li atoms ($r = 0.76$ Å) with respect to Si ($r = 0.26$ Å) and Fe atoms ($r = 0.78$ Å).[19] Li−O and Fe−O average distances are 2.153 Å and 2.156 Å, and the P−O average distance is 1.534 Å,[17] respectively.

On this basis, the preparation of our $Li_{1-x}Fe_{1+x}P_{1-x}Si_xO_4$ solution can simply be viewed as the replacement of Li by Fe in the M1 site with the associated substitution of P for Si in tetrahedral sites. The XRD diffraction patterns of the obtained powders are shown in Figure 2a. X-ray diffraction patterns for $x = 0.35$, 0.50, and 0.75 (see $x = 0.5$ in Figure 2c) and a neutron powder diffraction pattern for $x = 0.07$ (Figure 2b) were refined with the Rietveld method. In some cases small amounts of Fe_2SiO_4 and α-Fe were also detected and included in the refinement. The refinements proceeded by initially constraining the Li(M1)/Fe(M1) and P/Si ratios on the basis of the amounts of reactants used. In the neutron refinement, x was fixed to 0.07 because of its low value, but Li and Fe were allowed to exchange their positions. In XRD refinements the occupations of the Li/P and Si/Fe pairs were constrained with the same value and left to vary with $\sum SOF_{M1} = \sum SOF_{M2} = 1$. All atomic displacement factors were considered to be isotropic, and in the case of XRD data they were constrained for same type of atoms or the same Wyckoff positions. In all cases an anisotropic-sized model for platelet domains was used to model the profile of the peaks, and the background was also refined by atomic interpolation of selected points.

Regardless of the degree of substitution (x), the $Li_{1-x}Fe_{1+x}P_{1-x}Si_xO_4$ XRD samples were entirely indexed in the space group *Pnma* with lattice constants $a = 10.331(3)$ Å, $b = 6.001(3)$ Å, and $c = 4.700(2)$ ($V = 291.47$ Å^3) for $x = 0$ in good agreement with literature reports. The refined a, b, and c lattice parameters together with the unit cell volume (V) were found to increase continuously (Figure 3) upon increasing x to reach values for Fe_2SiO_4 close to those reported in the literature: while b and c cell parameters increase linearly, in agreement with Vegard's law, the a parameter increase is steeper in the first half of the solid solution domain. The main refined parameters are detailed in Tables 1 and 2, and the evolution of atomic distances versus the refined value of x in $Li_{1-x}Fe_{1+x}P_{1-x}Si_xO_4$ is shown in Figure 4 (atomic distances for $x = 1$ and $x = 0$ have been obtained from ref 20). The substitution of P for larger Si atoms results in a concomitant lengthening of the tetrahedron

(16) Birle, J. D.; Gibbs, G. V.; Moore, P. B.; Smith, J. V. *Am. Mineral.* **1968**, *53*, 807–824.
(17) Chen, J.; Whittingham, M. S. *Electrochem. Commun.* **2006**, *8*, 855–858.
(18) Chung, S. Y.; Choi, S. Y.; Yamamoto, T.; Ikuhara, Y. *Phys. Rev. Lett.* **2008**, *100*, 125502.
(19) Shannon, R. D. *Acta Crystallogr.* **1976**, *A32*, 751–767.

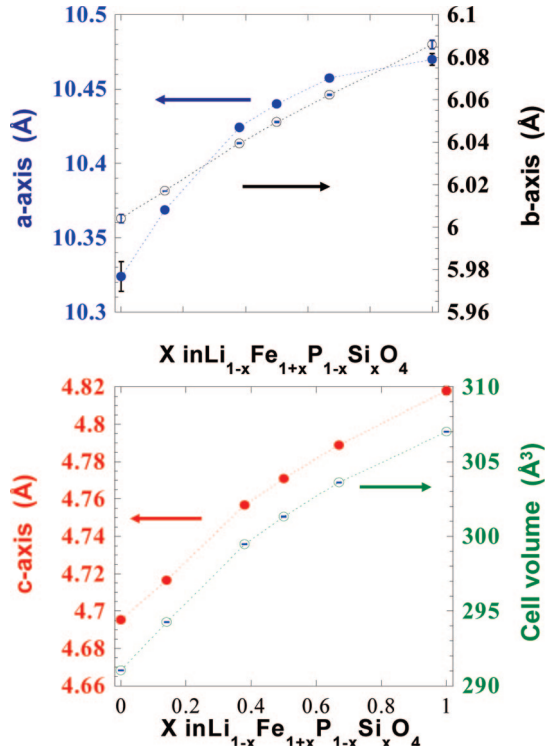

Figure 3. Unit-cell parameters as a function of x for various members of the $Li_{1-x}Fe_{1+x}P_{1-x}Si_xO_4$ series. Standard deviations have been corrected for local correlations according to ref 35.

bond lengths (Figure 4c). Despite the large standard deviations obtained in the bond lengths resulting from XRD refinements due to the fact that both Si and P are rather light elements, a clear tendency can be observed resulting in an increase of ~5% in all tetrahedron bond lengths, with increasing Si content. Although the substitution of Li for Fe atoms in M1 sites is not expected to induce major structural changes as their ionic radii are very similar, the edge sharing geometry of O2 and O3 with the tetrahedral sites causes larger O2−O3 interatomic distances resulting in the elongation of M1−O2 and M1−O3 bonds. In turn this elongation is compensated by a shrinkage of M1−O1 distances. In M2 all bonds are similarly elongated and, as in the starting structure, the longest bonds are still those corresponding to shared edges, to minimize cationic repulsions.

The composition of powder samples deduced from complementary chemical titration and nanoprobe EDS analysis is within ±5% away from the nominal composition $Li_{1-x}Fe_{1+x}P_{1-x}Si_xO_4$.

Effect of Synthesis Temperature on Phase Purity. Interestingly, we note a significant influence of the annealing temperature on the purity of the solid solution members. The phosphate-rich members can be obtained at lower temperatures (800−850 °C) than the lean ones (900−950 °C). At lower synthesis temperatures, the XRD patterns of the samples revealed splitting of the Bragg peaks suggesting the coexistence of two well-defined sets of reflections. Such phases were shown to be olivine-type phases with unit cell parameters slightly different from the end members, indicative of the coexistence of two solid solutions ($Li_{1-x'}Fe_{1+x'}FeP_{1-x'}Si_{x'}O_4$ and $Li_{1-x''}Fe_{1+x''}FeP_{1-x''}Si_{x''}O_4$) with x' and x'' depending on the initial value of x. For instance, nanoprobe EDS analysis together with TEM studies of two samples annealed at 850 °C and with nominal compositions $Li_{0.55}Fe_{1.45}P_{0.55}Si_{0.45}O_4$ and $Li_{0.65}Fe_{1.35}P_{0.65}Si_{0.35}O_4$ revealed the presence of multiple phases. The former (Figure 5a) contained 83% of the solid solution $Li_{0.66}Fe_{1.32}P_{0.66}Si_{0.33}O_4$ phase and 17% of the end member Fe_2SiO_4 phase. The latter (not shown) was composed of 93% and 4% of the $Li_{0.66}Fe_{1.32}P_{0.66}Si_{0.33}O_4$ and $Li_{0.33}Fe_{1.65}P_{0.33}Si_{0.66}O_4$, solid solution phases, respectively. The percentages are mathematically deduced by resolving the following equation: nominal composition = x(%) composition of phase A + y(%) composition of phase B. Needless to say, there are some errors in these percentage repartitions owing to uncertainties in the quantification of elements by EDS, which can reach ±5%, and the fact that the lithium amount was taken equal to the measured phosphorus amount.

We further explored this issue by monitoring the sample phase evolution as a function of temperature by XRD. To perform such measurements, a large sample of nominal composition $Li_{0.55}Fe_{1.45}P_{0.55}Si_{0.45}O_4$ was made, and equal amounts of powders were distributed in sealed stainless steel tubes that were heated to temperatures ranging from 700 to 980 °C, maintained at these temperatures for 24 h, and then rapidly cooled down. The XRD patterns of the recovered powders are shown in Figure 5b. Note that for such a composition, temperatures as high as 960 °C are needed to obtain single-phased samples. For lower temperatures, the XRD powder pattern shows the coexistence of two sets of Bragg peaks that were separately indexed in the space group *Pnma*. Regardless of the temperature up to 940 °C we note the coexistence of the Fe_2SiO_4 phase with a solid solution phase which lattice parameters varied as a function of the temperature. We could then deduce the composition (x) of the solid solution phase from Figure 3 and the temperature dependence of the unit cell volume; x varying from $x = 0.13$ to $x = 0.22$, 0.28, 0.35, 0.46 as T increases from 700 °C, to 800 °C, 850 °C, 900, and 940 °C, respectively. Upon further increasing temperature such phases were shown to merge into a single one, highlighting the importance of determining the right annealing temperature and annealing time for each member of the series.

Mössbauer Measurements. In addition to X-rays and neutron diffraction, Mössbauer spectrometry is a technique of choice to monitor Fe^{II} distribution variation as a function of x in the $Li_{1-x}Fe_{1+x}P_{1-x}Si_xO_4$ series owing to the fact that ^{57}Fe is an active Mössbauer probe. The Mössbauer spectra recorded at 300 K (Figure 6) for the various members of the $Li_{1-x}Fe_{1+x}P_{1-x}Si_xO_4$ series were analyzed for each member to extract the isomer shifts (δ) and quadrupole splitting values (Δ) (Table 3). The end members show the typical spectra of the olivine structures with, namely, the presence of a quadrupole doublet (δ= 1.21 mm/s, Δ= 2.95 mm/s), characteristic of Fe^{II} in the octahedral site, for the $x = 0$ (triphylite) phase,[20−24] and two quadrupole doublets with similar parameters (δ=1.13 mm/s, Δ= 2.72 mm/s; δ=1.16

(20) Yakubovich, O. V.; Simonov, M. A.; Belov, N. V. *Dokl. Akad. Nauk. SSSR* **1977**, *235*, 93–95.
(21) Li, Z.; Shinno, I. *J. Mineral.* **1997**, *19*, 99.
(22) Andersson, A. S.; Kalska, B.; Häggström, L.; Thomas, J. O. *Solid State Ionics* **2000**, *130*, 41–52.

Table 1. Lattice Constants and Rietveld Refinement Results for Samples with Theoretical Values of $x = 0.07$, 0.35, 0.5, and 0.75 in $Li_{1-x}Fe_{1+x}P_{1-x}Si_xO_4$

	$x = 0.07$	$x = 0.35$	$x = 0.5$	$x = 0.75$
radiation type	neutron (D1A, ILL)	X-ray	X-ray	X-ray
wavelength (Å)	1.91 (Å)	$\lambda_1 = 1.540530$ Å $\lambda_2 = 1.544310$ Å	$\lambda_1 = 1.540530$ Å $\lambda_2 = 1.544310$ Å	$\lambda_1 = 1.540530$ Å $\lambda_2 = 1.544310$ Å
a (Å)	10.36879(8)	10.4240(1)	10.4398(1)	10.4575(2)
b (Å)	6.01710(5)	6.03937(7)	6.04957(7)	6.06274(1)
c (Å)	4.71639(4)	4.75676(7)	4.77074(6)	4.78852(1)
V (Å^3)	294.256(4)	299.460(6)	301.303(6)	303.60(1)
Rp (%)	5.19	1.99	2.37	2.38
Rwp (%)	6.48	2.61	3.23	3.62
R Bragg (%)	5.15	6.39	5.84	5.35
Rexp (%)	5.33	1.58	2.15	1.31
χ^2	5.14	2.72	2.25	7.65

Table 2. Atomic Coordinates for Samples with Theoretical Values of $x = 0.07$, 0.35, 0.5, and 0.75 in $Li_{1-x}Fe_{1+x}P_{1-x}Si_xO_4$

atom	Wyck.	*x/a*	*y/b*	*z/c*	B_{iso} (Å^2)	SOF
		$0.07Fe_2SiO_4 + 0.93$ LiFePO$_4$				
Li (M1)	4a	0	0	0	2.2(8)	0.87(2)
Fe (M1)	4a	0	0	0	2.2(8)	0.13(2)
Li(M2)	4c	0.2823(1)	0.25	0.9777(4)	0.19(5)	0.06(2)
Fe (M2)	4c	0.2823(1)	0.25	0.9777(4)	0.19(5)	0.94(2)
P	4c	0.0965(3)	0.25	0.4182(6)	0	0.93(2)
Si	4c	0.0965(3)	0.25	0.4182(6)	0	0.07(2)
O(1)	4c	0.0978(3)	0.25	0.7474(6)	0.48(3)	1.00
O(2)	4c	0.4585(2)	0.25	0.2006(6)	0.53(2)	1.00
O(3)	8d	0.1663(2)	0.0459(3)	0.2877(4)	0.34(4)	1.00
		$0.35Fe_2SiO_4 + 0.65$LiFePO$_4$				
Li (M1)	4a	0	0	0	2.0(1)	0.594(3)
Fe (M1)	4a	0	0	0	2.0(1)	0.406(3)
Fe (M2)	4c	0.2816(1)	0.25	0.9826(5)	1.50(5)	1.0
P	4c	0.0967(3)	0.25	0.4261(5)	1.00(8)	0.594(3)
Si	4c	0.0967(3)	0.25	0.4261(5)	1.00(8)	0.406(3)
O(1)	4c	0.0954(5)	0.25	0.7454(9)	0.70(7)	1.0
O(2)	4c	0.4575(5)	0.25	0.2049(9)	0.70(7)	1.0
O(3)	8d	0.1649(5)	0.0451(6)	0.2920(7)	0.70(7)	1.0
		$0.5Fe_2SiO_4 + 0.5$LiFePO$_4$				
Li (M1)	4a	0	0	0	2.1(1)	0.506(3)
Fe (M1)	4a	0	0	0	2.1(1)	0.494(3)
Fe (M2)	4c	0.2810(1)	0.25	0.9850(4)	1.51(5)	1.0
P	4c	0.0977(3)	0.25	0.4260(5)	1.60(8)	0.506(3)
Si	4c	0.0977(3)	0.25	0.4260(5)	1.60(8)	0.494(3)
O(1)	4c	0.0944(6)	0.25	0.7507(8)	2.42(8)	1.0
O(2)	4c	0.459(5)	0.25	0.2037(9)	2.42(8)	1.0
O(3)	8d	0.1651(5)	0.0443(6)	0.2926(7)	2.42(8)	1.0
		$0.75Fe_2SiO_4 + 0.25$LiFePO$_4$				
Li (M1)	4a	0	0	0	2.6(3)	0.293(8)
Fe (M1)	4a	0	0	0	2.6(3)	0.707(8)
Fe (M2)	4c	0.2810(2)	0.25	0.9875(8)	1.4(2)	1.0
P	4c	0.0978(4)	0.25	0.4317(8)	1.4(1)	0.293(8)
Si	4c	0.0978(4)	0.25	0.4317(8)	1.4(1)	0.701(8)
O(1)	4c	0.0932(7)	0.25	0.756(1)	2.4(1)	1.0
O(2)	4c	0.4581(5)	0.25	0.208(1)	2.4(1)	1.0
O(3)	8d	0.1641(6)	0.0425(8)	0.295(1)	2.4(1)	1.0

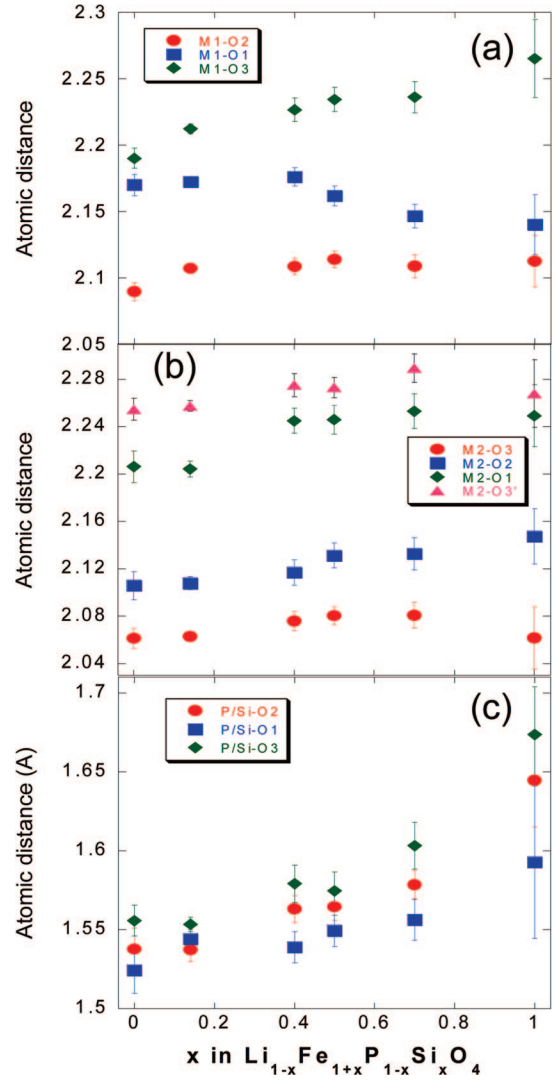

Figure 4. Evolution of atomic distances versus the refined value of x in $Li_{1-x}Fe_{1+x}P_{1-x}Si_xO_4$; within (a), (b), and (c) are the distances characterizing the M1, M2 and tetrahedral P site, respectively. Atomic distances for $x = 1$ and $x = 0$ have been obtained from refs 17.

mm/s, $\Delta = 2.94$ mm/s) of essentially equivalent contribution (45 and 48%, respectively), characteristic of two nonequivalent octahedral sites ($(Fe)_{M1}(Fe)_{M2}[Si]O_4$) for the $x = 1$ (fayalite) end member.[24,25] All the intermediate samples $0.15 \leq x \leq 0.75$ show very similar spectra with a broader and asymmetric quadrupole doublet, which as for the $x = 1$ member could be analyzed as being the sum of two doublets having similar δ and Δ parameters. The smooth and continuous changes in the isomer shifts and quadrupole splitting values through the series (Figure 7a,b, respectively) provide unambiguous evidence, as previously suggested from XRD measurements, for the existence of a complete solid solution based on the olivine structure of $(Li)_{M1}(Fe)_{M2}[P]O_4$, which can be represented as $(Li_{1-x'}Fe_{x'})_{M1}(Fe_{1-x''}Li_{x''})_{M2}[P_{1-x}Si_x]O_4$ with $x = x' - x''$ resulting in the overall formula

(23) Prince, A. A. M.; Mylswamy, S.; Chan, T. S.; Liu, R. S.; Hannoyer, B.; Jean, M.; Shen, C. H.; Huang, S. M.; Lee, J. F.; Wang, G. X. *Solid State Commun.* **2004**, *132*, 455–458.
(24) Hannoyer, B.; Prince, A. A. M.; Jean, M.; Liu, R. S.; Wang, G. X. *Hyperfine Interact.* **2006**, *167*, 767–772.
(25) Eibschütz, M.; Ganiel, U. *Solid State Commun.* **1967**, *5* (4), 267–272.

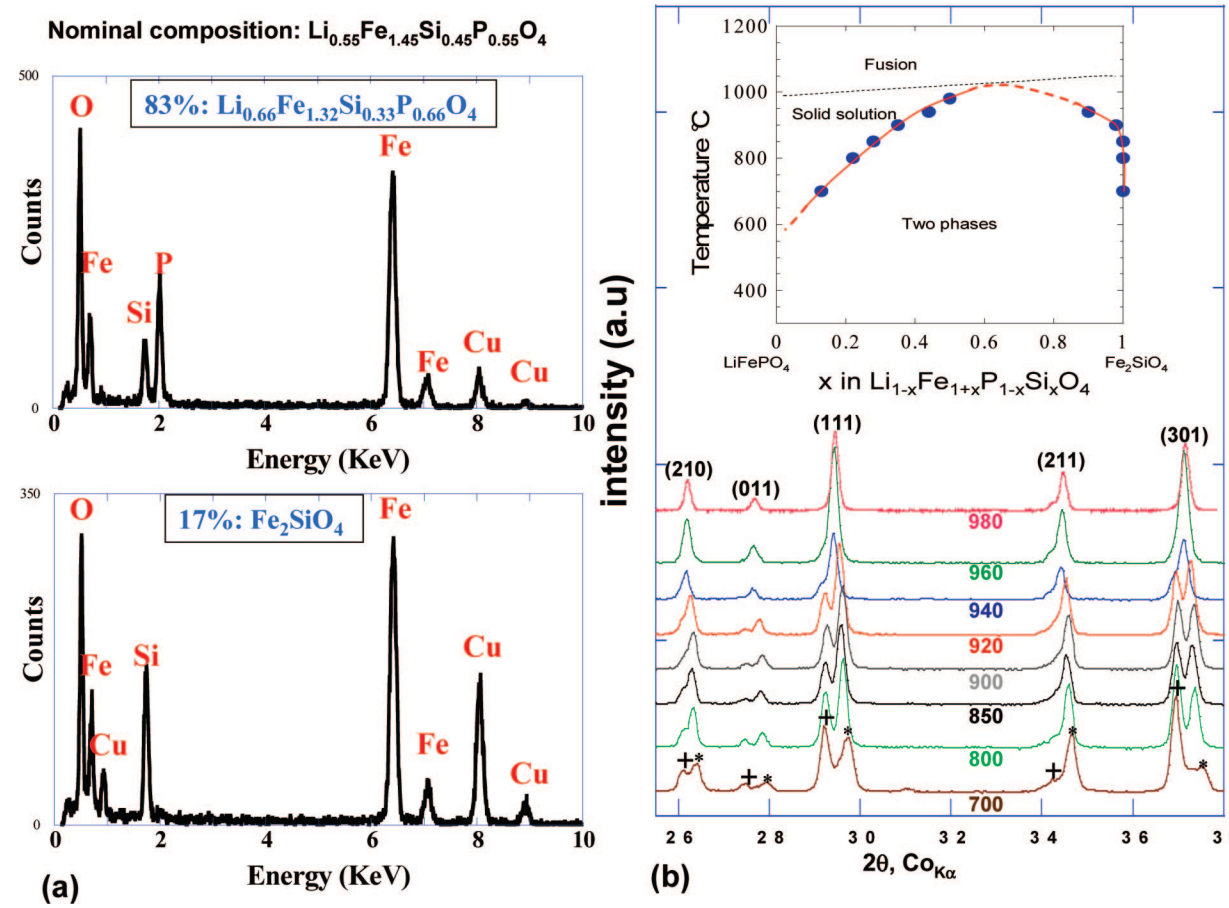

Figure 5. (a) Nanoprobe analysis for a sample of nominal composition $Li_{0.65}Fe_{1.35}P_{0.65}Si_{0.35}O_4$ annealed at 800 °C. The XRD powder patterns for samples of nominal composition $Li_{0.50}Fe_{1.50}P_{0.50}Si_{0.50}O_4$ annealed at various temperatures ranging from 700 to 980 °C are reported in (b); the top plot aims to illustrate the temperature dependence composition of the two end phases which merge to give a single phase at a higher temperature than 960 °C.

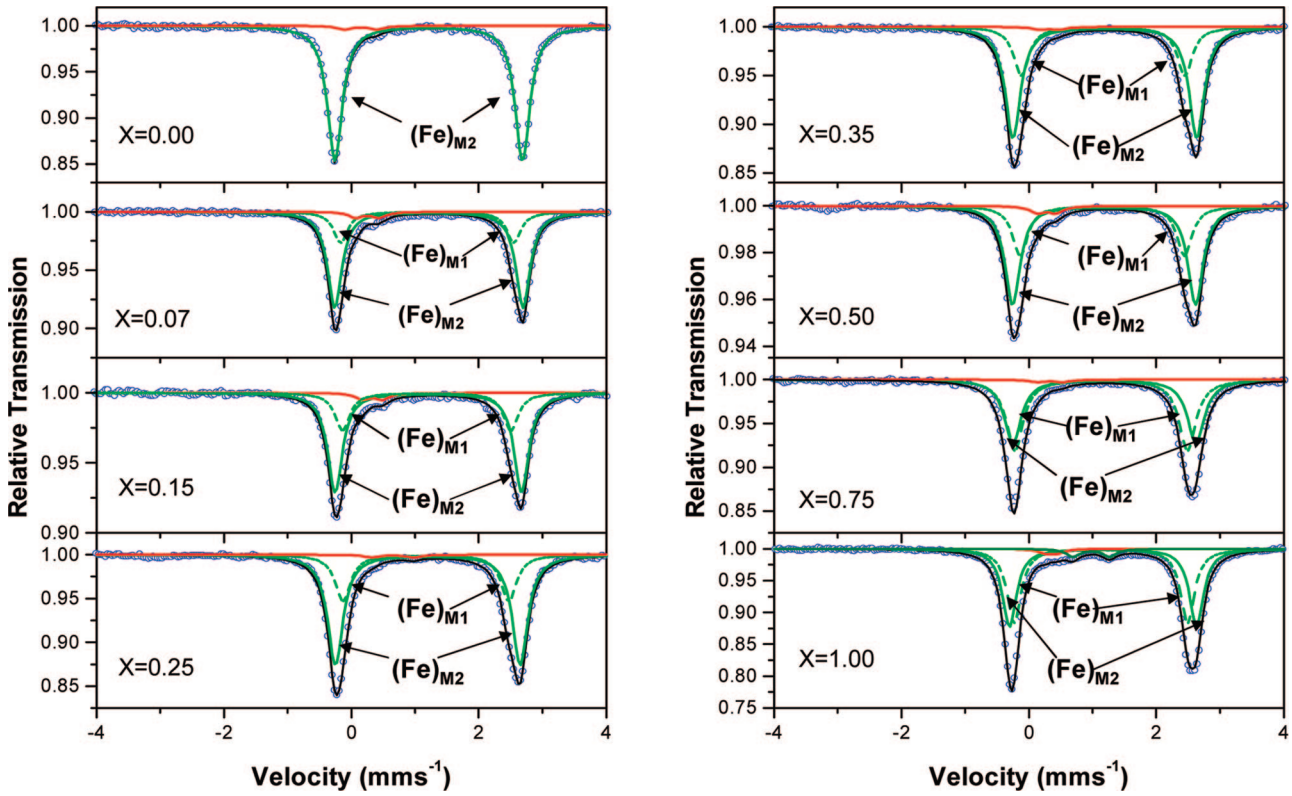

Figure 6. Mössbauer spectra for the various members of the $Li_{1-x}Fe_{1+x}P_{1-x}Si_xO_4$ series together with the deconvolution of the Mössbauer signal so as to highlight the different Fe sites.

Table 3. ^{57}Fe Mössbauer Data for Samples with $x = 0$, 0.07, 0.15, 0.25, 0.35, 0.50, 0.75, and 1.0 in $Li_{1-x}Fe_{1+x}P_{1-x}Si_xO_4$[a]

sample	δ (mm/s)	Δ (mm/s)	Γ (mm/s)	C (%)	attribution	$n(Fe)_{M1}$	$n(Fe)_{M2}$
$x = 0$	1.214(1)	2.946(8)	0.28(6)	97	$(Li)_{M1}(Fe^{II})_{M2}PO_4$	0	1
	0.14(4)	0.50(5)	0.28(6)	3	impurity Fe^{III}		
$x = 0.05$	1.244(4)	2.93(1)	0.26(2)	77	$(Fe^{II} + Li)_{M2}$	0.20	0.85
	1.15(2)	2.80(3)	0.26(2)	18	$(Fe^{II} + Li)_{M1}$		
	0.28(3)	0.26(3)	0.26(2)	5	impurity Fe^{III}		
$x = 0.07$	1.217(2)	2.957(9)	0.27(1)	72	$(Fe^{II} + Li)_{M2}$	0.26	0.81
	1.190(7)	2.72(1)	0.27(1)	23	$(Fe^{II} + Li)_{M1}$		
	0.51(2)	0.32(3)	0.27(1)	5	impurity Fe^{III}		
$x = 0.10$	1.214(4)	2.95(1)	0.26(1)	69	$(Fe^{II} + Li)_{M2}$	0.29	0.81
	1.18(1)	2.70(2)	0.26(1)	25	$(Fe^{II} + Li)_{M1}$		
	0.35(3)	0.28(3)	0.26(1)	6	impurity Fe^{III}		
$x = 0.15$	1.208(3)	2.925(9)	0.28(2)	69	$(Fe^{II} + Li)_{M2}$	0.31	0.83
	1.181(6)	2.64(1)	0.28(2)	26	$(Fe^{II} + Li)_{M1}$		
	0.22(4)	0.50(5)	0.28(2)	5	impurity Fe^{III}		
$x = 0.25$	1.199(2)	2.899(9)	0.30(1)	69	$(Fe^{II} + Li)_{M2}$	0.37	0.88
	1.169(4)	2.60(1)	0.30(1)	29	$(Fe^{II} + Li)_{M1}$		
	0.65(5)	0.65(6)	0.30(1)	2	impurity Fe^{III}		
$x = 0.35$	1.192(2)	2.885(9)	0.29(1)	68	$(Fe^{II} + Li)_{M2}$	0.41	0.94
	1.164(4)	2.57(1)	0.29(1)	30	$(Fe^{II} + Li)_{M1}$		
	0.32(5)	0.30(7)	0.29(1)	2	impurity Fe^{III}		
$x = 0.50$	1.181(2)	2.873(9)	0.29(1)	64	$(Fe^{II} + Li)_{M2}$	0.50	1.00
	1.153(4)	2.58(1)	0.29(1)	32	$(Fe^{II} + Li)_{M1}$		
	0.28(2)	0.29(3)	0.29(1)	4	impurity Fe^{III}		
$x = 0.75$	1.185(2)	2.874(9)	0.32(5)	47	$(Fe^{II} + Li)_{M2}$	0.91	0.84
	1.135(4)	2.711(1)	0.32(5)	51	$(Fe^{II} + Li)_{M1}$		
	0.39(6)	0.31(7)	0.32(5)	2	impurity Fe^{III}		
$x = 1.00$	1.163(4)	2.94(1)	0.27(4)	48	$(Fe)_{M1}(Fe^{II})_{M2}SiO_4$	1.00	1.00
	1.130(4)	2.72(1)	0.27(4)	45	$(Fe^{II})_{M1}(Fe)_{M2}SiO_4$		
	0.53(4)	0.55(5)	0.27(4)	2	impurity Fe^{III}		
	0.90(2)	0.74(2)	0.27(4)	5	impurity Fe^{II}		

[a] δ = isomer shift relative to α-Fe, Δ = quadrupole splitting, Γ = half-width at half-height, C = contribution to total absorption, $n(Fe)_{M1}$ and $n(Fe)_{M2}$ the number of Fe atoms on sites M1 and M2 calculated from C (see text).

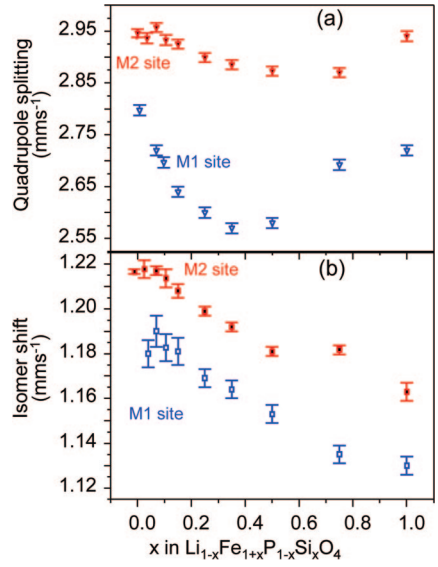

Figure 7. (a) Quadrupole splitting and (b) isomer shift extracted from the Mössbauer spectra in Figure 6 for the various members of the $Li_{1-x}Fe_{1+x}P_{1-x}Si_xO_4$ series.

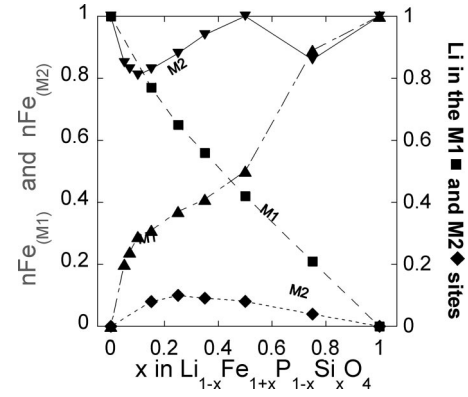

Figure 8. Cationic occupation of the M1 and M2 sites in the $Li_{1-x}Fe_{1+x}P_{1-x}Si_xO_4$ phases, as calculated from the deconvolution of the ^{57}Fe Mössbauer and the ^{7}Li MAS NMR spectra in Figures 6 and 9, respectively. The data can also be found in Tables 3 and 4.

$Li_{1-x}Fe_{1+x}P_{1-x}Si_xO_4$. Additional weak signals are seen on the Mössbauer spectra for all members of the series indicating the presence of impurities in the range of 2−5% containing either Fe^{III} or Fe^{II} species. Such impurities could not be identified owing to their exceedingly weak XRD signatures. Last, the Fe^{II} occupancy of the M1 and M2 sites could be extracted from the Mössbauer data. Such occupancy can be determined as described below by taking the $x = 0.07$ sample as an example. For this member of the series, based on the Fe nominal composition of 1.07, we can deduce that 0.23 and 0.72% of the Fe occupy the M_1 and M_2 sites, with the remaining 5% being ascribed to impurities, respectively. By mathematically removing the impurities, we estimate the effective occupancy of M_1 and M_2 sites to be $0.23/0.95 \times 100 = 0.24$ and $0.72/0.95 \times 100 = 0.76$, respectively. Once such a correction is made, the number of atoms in the M1 and M2 sites can be deduced as $0.24 \times 1.07 = 0.26$ and $0.76 \times 1.07 = 0.81$, respectively. Similar calculations were done for all the compositions, and the results are summarized in Table 3 (the last two columns) and shown in Figure 8. As expected, the Fe occupancy of the M1 site increases with increasing x in $Li_{1-x}Fe_{1+x}P_{1-x}Si_xO_4$. This contrasts with the Fe occupancy of the M2 site, which, to our surprise, decreases to 0.81 for $x = 0.07$ and then shows a wavy variation going back to 1 for $x = 0.5$, decreasing again to 0.85 for $x = 0.75$ prior to returning to 1 for $x = 1$. Such

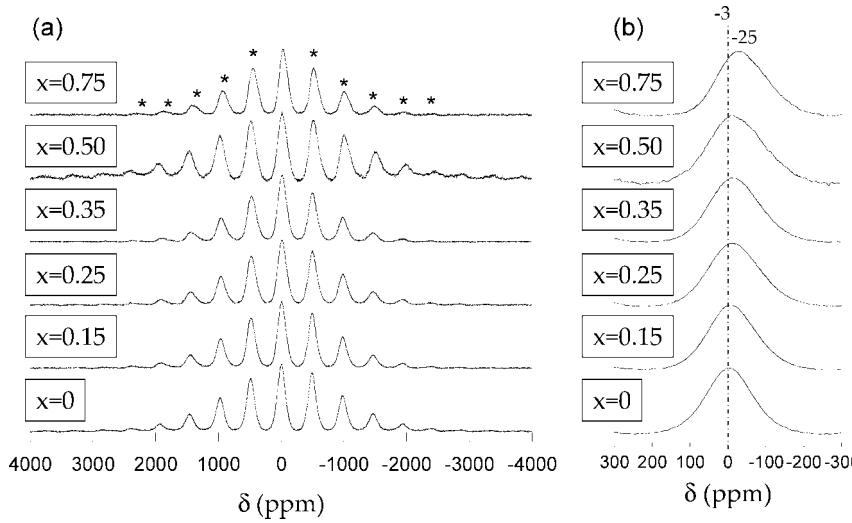

Figure 9. (a) ^{7}Li MAS NMR spectra of several $Li_{1-x}Fe_{1+x}P_{1-x}Si_xO_4$ phases (with x as indicated), acquired at 38 kHz. The spinning sidebands are marked with asterisks in the spectrum of the $x = 0.75$ sample. An expanded view of the isotropic resonances can be found in (b). The dashed line follows the displacement of the peaks with x and is provided as a guide for the eye. Relevant shift values are also indicated.

Table 4. Calculation of the Fractional Occupancy of Li in the M1 and M2 Sites Based on the M1:M2 Ratio (%Li in M1) Obtained from the Spectral Deconvolution of the ^{7}Li MAS NMR Spectra of $Li_{1-x}Fe_{1+x}P_{1-x}Si_xO_4$

x	theoretical $n(Li)_{M1}$	%Li in M1	experimental $n(Li)_{M1}$	experimental $n(Li)_{M2}$
0	1	100	1	0
0.15	0.85	90	0.77	0.08
0.25	0.75	87	0.65	0.10
0.35	0.65	86	0.56	0.091
0.50	0.550	84	0.42	0.081
0.75	0.25	83	0.21	0.04

The theoretical occupancy of Li in the M1 site, calculated assuming no cation mixing, is also given for comparison.

indirectly determined values should not be overinterpreted as they rely on the precise determination of the impurity phases and on the quality of the M1, M2 fits. Nevertheless, they convey the message that the dual Si/Fe substitution promotes cationic disorder/intersites mixing allowing the Li ions to occupy both M1 and M2 sites.

NMR Studies. ^{7}Li MAS NMR spectroscopy was performed to obtain insight into the distribution of lithium ions in the structure of the $Li_{1-x}Fe_{1+x}P_{1-x}Si_xO_4$ phases studied here. The spectra are dominated by broad peaks and a large spinning sideband manifold, indicative of the strong dipolar coupling of the lithium nuclear spins with the average magnetic moment of the paramagnetic Fe^{2+} ions (Figure 9a).[26] This interaction is sensitive to changes in the laying-out of the Fe^{2+} ions around the observed nucleus (lithium, in this case). No large variations were observed in our spectra, suggesting that the Li^+-O-Fe^{2+} interactions are similar in the different phases. The only exception is the $x = 0.50$ sample, where all the sidebands in this spectrum span a wider frequency range than seen in the other spectra. Given the fine-tuning of the synthesis conditions used to make pure samples, it is possible that the method employed for this specific sample results, to some extent, in slightly different structural features or different levels of magnetic (Fe_2O_3) impurities in the samples analyzed by NMR.

The isotropic peak values follow a clear and continuous trend to lower frequencies (i.e., lower ppm values) along the series (Figure 9a), again suggesting continuous solid−solution behavior. In addition, a shoulder to the right of this peak was found to appear for $x > 0$ and to grow as the iron and silicon contents increased. The resonances can be deconvoluted by combining two different peaks of similar width and Gaussian character, but with very different intensity. While the largest peak was clearly found to shift from −3 ppm at $x = 0$ to −26 ppm at $x = 0.75$, the weaker peak only shifted from −110 to −125 ppm from $x = 0.15$ to $x = 0.75$. However, given the significant overlap between the two signals, the shift values and relative intensities of the two peaks need to be treated with some caution. The fact that this new signal appears at more negative shifts in the ^{7}Li NMR spectra is consistent with the existence of only Fe^{2+} ions in the different compounds, since the presence of Fe^{3+} impurities in other $Li_xFe_yPO_4$ samples leads to new peaks at positive values.[27] Instead, the appearance and growth of a second resonance are correlated with the observation of cationic crystallographic site exchange by Mössbauer spectroscopy and consequent substitution of Li on the M2 sites. Thus, the stronger signal is ascribed to Li^+ ions in the M1 sites, as in $LiFePO_4$[28] ($x = 0$ in our study), whereas the shoulder at lower ppms is tentatively assigned to the presence of Li^+ ions in the M2 sites. On the basis of this assumption and the composition of each sample, a calculation of the percentage of lithium present in site M1 can be performed by using the deconvolution results (Table 4). A small but steady decrease in the percentage of Li occupancy on the M1 site of the $Li_{1-x}Fe_{1+x}P_{1-x}Si_xO_4$ phase is seen with x, which indicates that the tendency for Li to substitute for iron in the M2 site is slightly larger at the silicon-rich end of the phase diagram. The lithium occupation in each site was also

(26) Grey, C. P.; Dupré, N. *Chem. Rev.* **2004**, *104*, 4493–4512.

(27) Gibot, P.; Casas-Cabanas, M.; Cabana, J.; Hamelet, S.; Masquelier, C.; Grey, C. P. Manuscript in preparation.

(28) Tucker, M. C.; Doeff, M. M.; Richardson, T. J.; Finones, R.; Reimer, J. A.; Cairns, E. J. *J. Am. Chem. Soc.* **2002**, *124*, 3832.

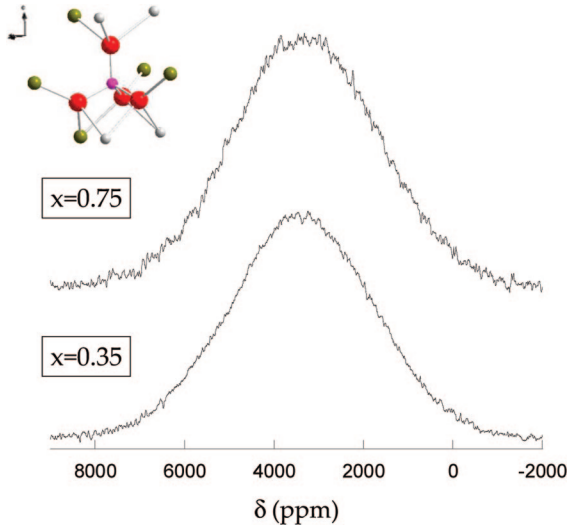

Figure 10. Sum of the ^{31}P MAS NMR spectra of $Li_{1-x}Fe_{1+x}P_{1-x}Si_xO_4$ with $x = 0.35$ and 0.75, acquired at different irradiation frequencies, separated by 650 kHz. Although a very high spinning speed of 38 kHz was used, no isotropic resonances could be resolved. A scheme of the first anionic and cationic coordination shells of the P/Si site is shown as an inset. The red balls depict oxygen ions, whereas the white and green balls depict ions in the M1 and M2 sites, respectively.

calculated and is plotted in Figure 8. As expected, this magnitude decreases linearly for the M1 site, as the occupation of iron increases, as shown by the Mössbauer results, resulting in, within error, a good correlation between the values obtained by these two methods. Interestingly, the amount of lithium in the M2 site is maximum when $x = 0.15-0.35$ and then decreases, as the overall concentration of Li^+ decreases. This provides further evidence for the existence of cationic disorder in the phases with intermediate compositions in the $Li_{1-x}Fe_{1+x}P_{1-x}Si_xO_4$ system.

The existence of an increasing amount of Fe^{2+} ions in the environment of Li^+ ions in the M1 site could explain the increase in absolute value of the shift of the resonance associated to this site, since the NMR shifts in paramagnetic materials are generally considered to be additive; that is, they increase with increasing amount of paramagnetic ions in the cation coordination sphere.[26] This argument cannot solely be used to explain the larger absolute value of the signal assigned to Li^+ ions in the M2 site (Li(M2)), since this site is surrounded by only four M2 cations, while the M1 site is surrounded by six, and thus has fewer Li(M2)−O−M2 interactions. Given that M2 is *predominantly* occupied by Fe, a larger shift is expected for Li(M1). One possible explanation for this higher shift of the resonance that we have assigned to Li(M2) is that the Fe^{2+} present in the M1 site as a result of both the iron excess and the cationic crystallographic mixing tends to be located close to the defects (Li) in the M2 site, thereby increasing the amount of transition metal ions in the coordination sphere of these lithium ions.

Additional information on the structural evolution of the phases prepared in this study was obtained from the ^{31}P NMR spectra of samples with $x = 0.35$ and 0.75 (Figure 10). Unfortunately, the interactions of these nuclei with neighboring Fe^{2+} ions are very strong and cannot be averaged by using very fast magic angle spinning (38 kHz). The result is a spectrum with very broad lines, where there is no resolution of the isotropic resonance. Nonetheless, changes in the local environment of phosphorus in the compound should still lead to variations of these broad signals. This is not the case here, as both spectra show a large symmetric peak around 3400 ppm and with a similar width. Similar results were obtained by performing static ^{31}P NMR on a sample of pure $LiFePO_4$ [29,30] indicating that the phosphorus environment in both samples is not only maintained along the series but also remains very close to that of pure $LiFePO_4$. One plausible explanation is that the iron content in both the M1 and M2 sites in these environments (Figure 10, inset) does not change even in phases closer to the end member, Fe_2SiO_4, and that there is a tendency to the formation of $LiFePO_4$-like clusters in the structure of all these compounds. These clusters would most probably be small and disordered, given the lack of superstructure peaks in the diffractograms, which can all be indexed using a simple olivine-type cell with *Pnma* space group. First principle calculations are being presently conducted to test the feasibility of this clustering model.

The existence of $LiFePO_4$-like (and, consequently, Fe_2SiO_4-like) clustering in the phases could also be a factor leading to a larger absolute value of the ^{7}Li NMR shift of the Li^+ in the M2 sites with respect to those in M1. The shorter distance of the P−O bond with respect to that of Si−O, together with the higher charge of phosphorus versus silicon, is expected to result in a slightly more covalent Fe−O−P interaction in comparison to Fe−O−Si. This, in turn, would result in a weaker transfer of spin density from iron to lithium through oxygen in phosphorus-rich regions, thus producing lower absolute shift values. Therefore, the larger shift values observed for ^{7}Li in the M2 sites could be related to the Li^+ ions in the M2 site being closer to $[SiO_4]$ units rather than $[PO_4]$.

Since both NMR and Mössbauer provided evidence for the presence of some intersite mixing, we attempted to investigate this disorder in our XRD refinements but without too much success as the weak contribution of Li to the X-ray diffraction pattern allows only Fe substitution in M1 site to be considered and in turn the refinement of such fine structural details occurring in low amounts requires very high quality data. A similar approach was undertaken to refine the neutron diffraction pattern collected for the $x = 0.07$ sample as ND is more sensitive to lithium occupancies than XRD. In this case the intersite mixing converged to a small amount of intersites (ca. 6 %), in agreement with the Li occupancies obtained by NMR for similar compositions, confirming thus the presence of small amounts of Fe/Li disorder in our samples.

Electrochemical Measurements. The electrochemical performances of $LiFePO_4$ electrodes are known to be limited by their low intrinsic electronic/ionic conductivity. It is only through particle size reduction coupled with smart processing, namely, carbon nanopainting, that a material that would have been otherwise disregarded was turned into an attractive electrode material. [8] Needless to say that our high synthesis temperature conditions favor coarse rather than nanoparticles,

(29) Kim, J.; Shirakawa, J.; Grey, C. P., submitted for publication.
(30) Becker, K. D. *Solid State Ionics* **2001**, *141−142*, 21–30.

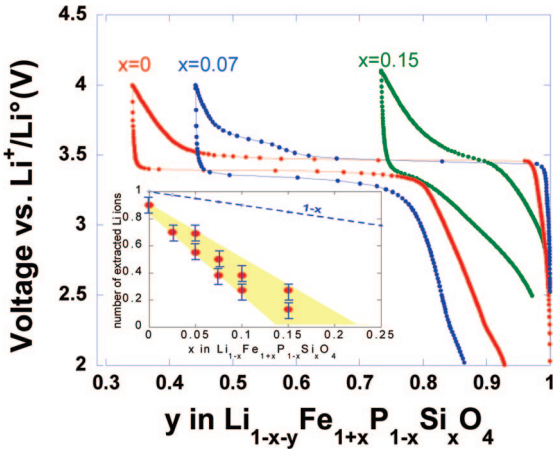

Figure 11. Charge/discharge galvanostatic curves at C/10 ($1Li^+$ in 10 h) for Li half-cells, using the early members of the $Li_{1-x}Fe_{1+x}P_{1-x}Si_xO_4$ series as the positive electrodes. The inset shows the deviation from the expected $(1-x)$ Li capacity ab, the measured as deduced electrochemical.

explaining the poor electrochemical activity of our as-made samples. To recover such an electrochemical activity (as seen in Figure 11) our samples were first ball-milled for 30 min in a Spex-800 apparatus and then carbon-coated via the pyrolysis of C-based polymers. The amount of carbon coating equates 3% as deduced from thermal gravimetric analysis (TGA) measurements done under oxygen. Similar treatments were performed on all members of the $Li_{1-x}Fe_{1+x}P_{1-x}Si_xO_4$ series. We note that the sample electrochemical activity does not vary as $(1 - x)$ as expected upon increasing the Si substitution but rather rapidly decays so that beyond the composition $x = 0.20$ no sign of electrochemical activity could be detected. With increasing x, the reversible capacity rapidly decreases and the polarization increases. Among the two possibilities to account for such decay are (1) a decrease in the sample electronic/ionic conductivity caused by the dual substitution and (2) the presence of Fe atoms on the Li sites, which presumably prevents the diffusion of the Li ions down the channels in the structure, hence leading to a poor performance.

Discussion

When looking back, the feasibility of preparing a complete solid solution does not come as a real surprise since both end members $LiFePO_4$ and Fe_2SiO_4 have the same structure. Thus, why had such a solid solution never been reported before? The answer lies in its synthesis procedure and mainly in the choice and nature of the precursors, with SiO_2 being the most problematic. Attempts to prepare the solid solutions by simply reacting the following reaction components $[(1 - x)LiFePO_4 + x[(2/3)Fe_2O_3 + (2/3)Fe + SiO_2]$ were unsuccessful owing to rapid temperature-driven crystallization/coarsening of Sio_2,[31,32] before it could react with the other components, regardless of the annealing temperature. Hence the motivation to prepare Fe_2SiO_4 according to the reaction $(2/3)Fe_2O_3 + (2/3)Fe^0 + SiO_2 = Fe_2SiO_4$. Unless highly divided SiO_2 particles (5 to 10 nm) are used, this reaction will fail because of competing reactions, which will lead to impurity phases, again highlighting the importance of particle size as an extra parameter in addition to composition, structure, temperature, and pressure to control specific reaction paths.

Once the importance of the SiO_2 particle size was identified, the complete solid solution could be made by various heating process sequences, enlisting either sealed stainless steel tubes or covered graphite crucibles for flash heating. For the former, particular attention must be given to the type of stainless steel used as we experienced that Cr-rich stainless steel was also detrimental to phase purity owing to the highly reducing character of Cr, leading to the decomposition of Fe_2SiO_4 into $SiO_2 + Fe^0$. The latter process is obviously associated with a risk of Fe oxidation, and therefore such an effect is counterbalanced by using a reacting vessel made of reducing material (carbon). Owing to such competing oxidation−reduction reactions, the process must remain short to prevent the oxidation from taking over, the reason why flash heating is preferred. Longer reaction times would always lead to oxidized phases.

Finally, although the two reaction processes were associated with differences in sample cooling rates (quenched for samples made in graphite containers as opposed to natural cooling for stainless or iron tubes), we did not observe noticeable effects on the final products (same lattice parameters), with the exception of subtle variations in the relative intensities of the Bragg peaks, most likely associated to different degrees of intersites mixing. We did, however, notice a significant influence of the annealing temperature on the purity of the solid solution members. The silicon-rich samples required higher temperatures than the phosphate rich samples to achieve complete solid solutions, two phases ($Li_{1-x'}Fe_{1+x'}FeP_{1-x'}Si_{x'}O_4$ and $Li_{1-x''}Fe_{1+x''}FeP_{1-x''}Si_{x''}O_4$) being observed for lower synthesis temperatures.

Turning to the electrochemical data, such dual substitution turns out to be detrimental to the performance of $LiFePO_4$ in terms of reversible capacity and polarization. Note that the decrease in capacity for $Li_{1-x}Fe_{1+x}P_{1-x}Si_xO_4$ does not scale with the total amount of $(1 - x)$Li as expected but decreases much faster, reaching 0 for $x = 0.20$. In light of both Mössbauer and NMR results, which have shown the presence of Fe into the M1 sites and of Li into the M2 sites, this does not come as a total surprise as years of cumulative experience on bulk materials have taught us that the presence of Fe atoms on the Li sites will presumably prevent the diffusion of Li ions down the channels in the structure and thus lead to poor electrode kinetics (i.e., limited capacity). An important limiting factor in the $Fe_{1+x}P_{1-x}Si_xO_4/Li_{1-x-y}Fe_{1+x}P_{1-x}Si_xO_4$ electrochemical reaction may also arise from the ionic and/or electronic transport within the particles $Li_{1-x}Fe_{1+x}P_{1-x}Si_xO_4$ themselves. From AC impedance, we could determine conductivity values of 0.95×10^{-9} S cm^{-1} for the pure $LiFePO_4$ in close agreement with previously reported literature values (1.39×10^{-9} S cm^{-1}). Such values were found to decrease rapidly with increasing Si substitu-

(31) Parise, J. B.; Yeganeh-Haeri, A.; Weidner, D. J.; Jorgensen, J. D.; Saltzberg, M. A. *J. Appl. Phys.* **1994**, *75*, 1361.
(32) Baur, W. H. *Acta Crystallogr., Sect. B* **1977**, *33*, 2615.
(33) Islam, S. M.; Driscoll, D. J.; Fisher, C. A.; Slater, P. R. *Chem. Mater.* **2005**, *17*, 5085.

tion, to the point that we could not determine their exact values with our present HP 4192A LF frequency analyzer. At first, as the dual Fe/Si substitution for Li and Fe preserves the Fe^{2+} valence state, little difference should be expected for the electronic conductivity of the Si-bearing samples with the exception of diffusion hindrance. Within this context, Maier's recent theoretical studies of Al/Si doping at the M1 site in $LiFePO_4$ bears some relevance.[33] On the basis of theoretical calculations, the authors have reported that substituting Fe^{2+} for either a trivalent (Al) or tetravalent (Si) cations within the $LiFePO_4$ framework results in an increase in the ionic conductivity owing to the fact that the dopants act as donors, hence increasing the Li vacancies. Simultaneously the number of holes should decrease as the ($Vac_{Li} \times h^{\circ}$) product should remain constant, thus leading to a decrease in the electronic conductivity. Such opposite changes in both electronic and ionic conductivity contrast in our substituted samples as both AC and DC measurements qualitatively show a decrease in both electronic and ionic conductivity. Besides the fact that the substituted Si atoms will not sit in an octahedral environment (a situation quite unlikely to occur with Si), another possibility for such a difference could be rooted in the nonvalidity of the proposed doping theory for contents extending beyond 2.5%.

(34) Maier, J.; Amin, R. *J. Electrochem. Soc.* **2008**, *155* (4), A339−A344.

Conclusions

We have reported the first breach into the "intangibility" of the anionic lattice in $LiFePO_4$ by preparing the complete $Li_{1-x}Fe_{1+x}P_{1-x}Si_xO_4$ solid solution ($x \leq 0 < 1$). Via complementary XRD, Mössbauer, and NMR measurements we showed that such a dual Fe and Si substitution triggers substantial antisite defects with some Li moving from the M1 to the M2 site and Fe from the M2 to the M1 site. Such defects were shown to be detrimental to the materials electrochemical performances, which rapidly decay from 160 mA h/g for $x = 0$ to 0 for x values approaching 0.20. Although such a study did not lead to better electrode materials, it unveils yet another attractive facet of $LiFePO_4$ chemistry that is far richer than initially expected and that we are presently exploring.

Acknowledgment. The authors wish to thank Christian Masquelier and Charles Delacourt for stimulating discussions regarding crystallography and transport measurements data. C.P.G. and J.C. thank J. Shirakawa for his help in the earlier stages of this project and for support from the Assistant Secretary for Energy Efficiency and Renewable Energy, Office of Freedom CAR and Vehicle Technologies of the U.S. Department of Energy under Contract No. DE-AC03-76SF00098, via Subcontract No. 6517749 with the Lawrence Berkeley National Laboratory.

CM801817N